

A model for cerebral ischaemia from gaseous emboli.

J.P. Hague ¹, C. Banahan ² and E.M.L. Chung ³

¹ Department of Physical Sciences, The Open University, Walton Hall, Milton Keynes, MK7 6AA, UK

² Medical Physics Department, Leicester Royal Infirmary, University Hospitals of Leicester NHS trust, LE1 5WW, UK

³ Department of Cardiovascular sciences, University of Leicester, Leicester LE3 9QP, UK

Abstract. The effects of bubbles on the cerebral bloodflow are difficult to quantify. We present a model to calculate how cerebral ischaemia is caused by deformable gaseous emboli. The model takes into account realistic adhesion forces, fluid dynamical considerations, a realistic parameterisation for the rate of bubble dissolution and the effects of buoyancy. We find that neglecting deformability of bubbles leads to a vast overestimation of ischaemia. The inclusion of buoyancy effects reduces the proportion of the vasculature that becomes compromised, but increases blockage times, thus lowering the risk of transient ischaemia but increasing the potential for focal injury. We also investigate the number and size of bubbles in a sudden shower of emboli that leads to persistent ischaemia capable of neuronal injury. Finally we investigate mitigation techniques such as insufflation of the operative area with CO₂ and alterations in arterial pressure.

1. Introduction

Neurological symptoms arising from clinical sources of embolisation can be expected to vary considerably depending on embolus size, composition and prevalence [Chung et al., 2007]. Large solid emboli (consisting of plaque or thrombus) usually form in the heart or large arteries such as the aorta or carotid, and once released into the circulation can have devastating consequences, travelling through the blood stream to become lodged in smaller arteries supplying the cortex. Embolisation can be asymptomatic, or lead to a spectrum of neurological disorders ranging from a subtle decline in neuropsychological function, or transient ischaemic events (such as decompression sickness), to pronounced focal deficits characteristic of severe stroke.

During invasive procedures such as open heart surgery, patients typically experience thousands of gaseous emboli with various clinical implications [Rodriguez et al., 2005, Moody et al., 1990]. Bubbles can also be observed in other scenarios as a cause of decompression sickness [Barak and Katz, 2005] and in patients fitted with mechanical heart valves [Georgiadis et al., 2005]. Depending on the number, size and embolisation

rate, embolisation of bubbles clearly produces various sequelae and it is the aim of this work to understand where the boundaries between symptoms occur.

To attempt to understand the outcomes from these varied sources of embolisation in a universal way, we previously introduced a model for the forecast of ischaemic stroke [Chung et al., 2007, Hague and Chung, 2009]. In that model, emboli were assumed to be rigid, and therefore to block any vessels of similar size. The model also assumed that all pressure was dropped over the arterioles and the flow at any bifurcation was determined only by the number of arterioles receiving flow downstream of the bifurcation. Our stroke model was used to discuss various clinical scenarios of embolisation, and revealed a nonlinear relationship between embolus properties and cerebrovascular blockages [Chung et al., 2007]. Previous clinical studies of embolisation revealed a positive correlation between embolus prevalence and adverse clinical outcome during some stages of surgery, but in many clinical situations the presence of emboli alone is insufficient to provide a reliable indicator of stroke risk [Omar et al., 2006, Brown et al., 2000, Stroobant et al., 2005].

There are a number of differences between solid emboli (which may be almost incompressible) and gaseous emboli which compress easily [Branger and Eckmann, 1999], that have potential to affect the locations in the vasculature where emboli become lodged. Gaseous emboli have a propensity to split and deform as they move through the vasculature and only block arteries when the surface area in contact with the walls becomes sufficiently large to oppose motion through stiction (Suzuki and Eckmann [2003]), whereas solid emboli block arteries when they encounter vessels of similar size. There is another significant difference between solid and gaseous emboli, which is their high buoyancy compared to thrombus which is approximately neutrally buoyant in the blood. Therefore a number of extensions are needed to properly model the motion of gaseous emboli through the vascular tree: (1) the emboli should be deformable (2) an approximation for stiction should be included, (3) an iterative fluid dynamical analysis is required to estimate the pressure drop in the whole tree, and (4) in a 3D vasculature an estimate of buoyancy effects would be useful.

In this paper, we discuss an extended model which includes features of gaseous emboli such as buoyancy and deformation. We start by introducing an extended stroke forecast model (section 2) and then present detailed results for prediction of transient and permanent ischaemic injury caused by showers of gaseous emboli, contrasting the results with those for solid emboli, and probing the effects of buoyancy (section 3). A summary can be found in section 4.

2. Model

2.1. Gaseous emboli

Gaseous emboli differ from solid thrombus and plaque since they are deformable, and also dissolve at a faster rate. By fitting to *in vivo* data from Branger and Eckmann

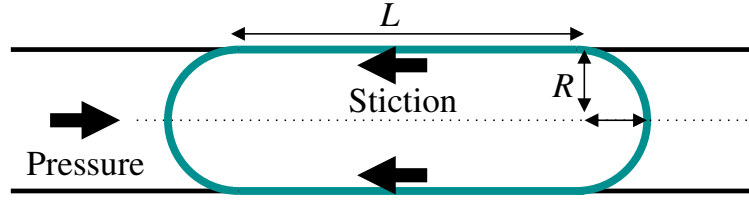


Figure 1. Schematic of a deformable embolus and forces leading to stiction

[1999] it becomes possible to parameterise the rate of embolus dissolution, yielding the following function:

$$V(t) = c(a - t)^b \quad (1)$$

where the volume at $t = 0$ corresponds to an embolus of size $V(0) = 2.8$ nl. The parameters for an air embolus are $a = (V(0)/c)^{1/b}$ minutes (which is the lifetime of a 2.8 nl embolus), $b = 2.00539 \pm 0.04699$ and $c = 0.00463395 \pm 0.0008206$ nl/min^{*b*}. CO₂ emboli dissolve around 20 times faster (Chaudhuri and Marasco [2011]) so (representing CO₂ parameters as primed variables) $c' = 20^b \times c$, $b' = b$ and $a' = (V(0)/c')^{1/b}$.

In order to consider deformability and stiction we assume that a gaseous embolus in a vessel of similar size deforms to a sausage-like shape (shown schematically in figure 1). This shape is a common finding in the arteries of patients following cardiac surgery, where autopsy reveals large numbers of sausage-like arteriole dilatations (Moody et al. [1990]). The surface area of the embolus touching the side of the vessel is computed by correcting for a domed end with the same radius as the vessel. The length of the cylindrical part of the embolus is $L = (V_{\text{emb}} - 4\pi R_{\text{vessel}}^3/3)/\pi R_{\text{vessel}}^2$, and the surface area touching the side is $2\pi R_{\text{vessel}}L$.

An embolus will stop moving when the pressure drop over a stationary embolus is insufficient to overcome stiction, i.e. $\Delta p/\pi R_{\text{vessel}}^2 < 2K(V_{\text{emb}} - 4\pi R_{\text{vessel}}^3/3)/R_{\text{vessel}}$. The coefficient of stiction has been measured, and is $K = 10\text{Nm}^{-2}$ (Suzuki and Eckmann [2003]). The pressure drop for the stationary embolus is equal to the difference between the pressure at the bifurcation upstream from the embolus and the capillary network (since the blood in vessels downstream of the embolus is not moving, and therefore there is no additional pressure drop over the downstream vessels).

The need to assign values to the pressures at bifurcations in the arterial tree is an added complication of dealing with deformable gaseous emboli, and means that at least a basic fluid dynamical analysis of flows in the tree is needed. This will be discussed below.

2.2. Bifurcating tree

The assumption of a bifurcating tree is justified by the analysis of high-resolution images of the human cortex (Cassot et al. [2006]) which show that 94% of branches in the cerebral vasculature consist of bifurcations ‡.

‡ Of the remaining nodes, 4% are trifurcations, 1% simple nodes and 0.5% have 4 or more daughters

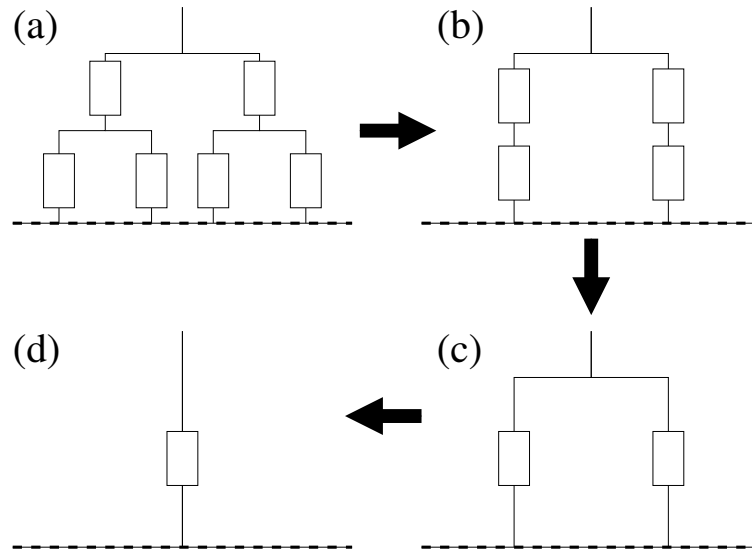


Figure 2. Schematic of the recursive procedure for computing pressures, flows and resistances.

2.3. Fluid dynamics and recursive computation

When considering the stiction of gas bubbles, it is essential to know the pressure drop across the embolus. Since the bifurcating tree in the model has a very large number of nodes, and the pressures need to be computed whenever an embolus moves, it is essential that a simplified fluid dynamics scheme is used so that the computational time is not excessive. We treat the fluid flow through the tree as Poiseuille flow. The pressure drop and effective resistance can be treated using electrical circuit analogues. Thus, parallel resistances can be rewritten as a single resistor, and this can be repeated recursively up the tree from the end arterioles to the parent node to compute all flows and pressures as an order N operation, where N is the number of vessels in the tree. This process is summarised in figure 2, and leads to rapid computations which are far faster than using matrix inversion or by directly solving simultaneous equations. In the following, the root node radius of the tree is 1mm.

Panel (a) shows the initial bifurcating tree. In panel (b), the smallest vessels have been rewritten as a single resistance. In panel (c) the resistances in series have been simplified, and in panel (d) the recursive step has been applied to the tree that resulted in (c). Clearly this procedure can be applied to any size of bifurcating tree. It is a simple matter to compute all flows and pressures at step (b) as there is effectively a potential divider in each branch at that stage. During the recursive procedure, these flows and pressures are stored, and the stored pressures and flows can be used for all calculations until any new blockages are introduced or existing blockages are freed as emboli dissolve.

2.4. Buoyancy

The effects of buoyancy are emulated by introducing preferential directions at bifurcations. An additional weighting, $w_A = (1 + A_g \cos(\theta))/2$ is included in the weighted probability to account for buoyancy. This type of weighting is consistent with the results in Eshpuniyani et al. [2005]. Once the additional weighting factors are introduced, the probability that an embolus travels in direction A at a bifurcation is,

$$P_A = w_A f_A / (w_A f_A + w_B f_B) \quad (2)$$

with $P_B = 1 - P_A$ and where f_A (f_B) is the flow in the a (b) direction. A_g is a parameter which is varied between 0 and 1, with $A_g = 0$ representing no correction due to buoyancy (where $w = 1/2$ as in the previous version of the model) and $A_g = 1$ an extreme correction. We note that this form for the weighting is *ad-hoc*, but we believe that it contains the essence of the corrections that will occur when emboli are buoyant. In this work we will use it as a tuning parameter to understand some features of buoyancy and future work will measure the precise form of the probabilities for a wide range of flow ratios. In this work, θ is a random parameter assigned to each bifurcation at time $t = 0$ to each instance of the ensemble, but in future work it will be the angle established from *in-silico* tree growth. Incidentally, this form may also mimic more realistic bifurcating trees, where large trunks have small branches.

2.5. Algorithm

The algorithm begins by calculating flows, pressures and resistances for an empty tree (using the procedure in section 2.3). It then proceeds as follows:

- (i) On any time step, an embolus may be created in the root node of the tree with probability $P_\tau \Delta\tau$ with size randomly chosen between 0 and r_{\max} . Here P_τ is the probability per unit time to create an embolus and $\Delta\tau = 1s$ is the length of the time step.
- (ii) All emboli dissolve leading to a reduction in radius during each time step according to the parameterisation in Sec. 2.1. Completely dissolved emboli are removed from the simulation. If the reduction in radius causes a change in the blockage state of the tree, flows and pressures are calculated again.
- (iii) The emboli move according to the following rules:
 - (a) If the pressure behind the deformed embolus is insufficient to overcome the stiction force exerted by the embolus (according to the theory in section 2.1) it does not move.
 - (b) If all arterioles downstream are blocked, the embolus may not move since there is no flow.
 - (c) If the embolus is smaller than the current node, and there is flow downstream.
 1. The flows in directions A and B are determined by solving the simplified fluid dynamics.

2. The embolus then moves in direction A with probability $P_A = f_A w_A / (f_A w_A + f_B w_B)$. Otherwise, it moves in direction B.

3. Results

Here, we investigate total blockage, and the percentage of arterioles blocked for at least 5 minutes, 10 minutes and 15 minutes as these are the timescales over which we expect neuronal changes to occur. As part of these simulations the size range of incoming emboli, buoyancy, the total number of emboli in a shower, and the rate of embolisation are varied. We also investigate the difference between deformable gaseous emboli and non-deformable solid emboli. Embolisation starts at time $t = 10$ s and finishes after the number of emboli to be explored has been delivered. The embolisation is steady, and occurs at a rate of 1/s and 0.5/s. In this way, we can determine if a short period of rapid embolisation is more damaging than chronic embolisation over a longer period. In clinical scenarios, the embolisation rate can be higher than this, but it becomes difficult to differentiate between multiple emboli. For embolisation showers which have a significantly shorter time duration than the embolus dissolve time, the outcome from the showers is expected to be similar. An ensemble of 100 simulations is generated, with the weighting coefficients for buoyant emboli chosen randomly in each instance.

Figure 3 shows the percentage of nodes blocked on each timestep. In the simulations shown, emboli have sizes ranging between 0 to 0.5 mm. As in our original model (Chung et al. [2007]), after embolisation begins the proportion of blocked nodes quickly reaches a dynamic equilibrium where as many emboli are dissolving and leaving the system as entering the vasculature. There is a small difference between the height of the plateau as buoyancy effects are turned on in the simulation. Buoyancy effects reduce the proportion of blocked nodes because certain paths through the tree become more probable if the emboli are buoyant. Once embolisation stops, the emboli rapidly dissolve and blockages are cleared.

There is a major difference between the percentage of blocked end arterioles when emboli are assumed to be deformable and rigid. If emboli are assumed to be rigid, the proportion of blocked nodes rapidly increasing to 100% for the parameters shown. In contrast, approximately 5% of end arterioles become blocked when deformable emboli are introduced into the model. This shows that deformability must be taken into account in models of gaseous embolisation.

Knowledge of the percentage of instantaneous blockages is of limited diagnostic use, since it does not contain any information about the length of time that a particular arteriole has received zero flow. If flow is absent for a sufficiently long time, neuronal changes begin to occur (<1 min) and surrounding tissue becomes ischaemic (<5 mins). Eventually these changes become irreversible leading to necrosis and cerebral infarcts. Therefore, we also measure the proportion of nodes that have been ischaemic for at least 5 minutes, 10 minutes etc.

An estimate for the number of nodes that have been ischaemic for at least 10 minutes

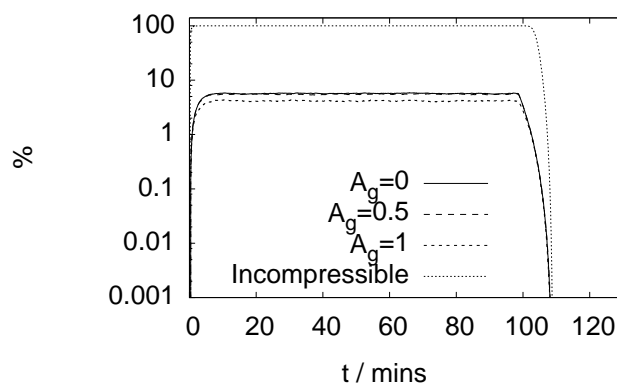


Figure 3. Percentage of nodes blocked vs time giving an indication of transient effects. After embolisation begins the proportion of blocked nodes quickly reaches a dynamic equilibrium where as many emboli are dissolving and leaving the system as entering the vasculature. There is a small difference between the height of the plateau as gravitational effects are turned on in the simulation, and gravitational effects also reduce the proportion of blocked nodes because certain paths through the tree become more probable if the emboli are buoyant. Once embolisation stops, the emboli rapidly dissolve and total blockage returns to zero. N.B. The graph is plotted on a logarithmic scale.

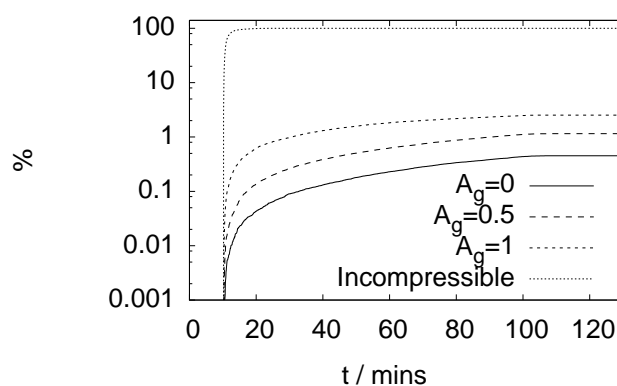


Figure 4. Percentage of individual nodes compromised for at least 10 minutes vs time. Again several values for the coefficient A_g are shown, and the results for non-deformable emboli are included for comparison. The proportion of nodes that have been ischaemic for at least 10 minutes at some time during the simulation increases monotonically with time and the number of emboli in the shower. It should be noticed that these proportions do not increase linearly, presumably because the same nodes can become ischaemic at a later time in the simulation. This non-linearity is particularly clear for $A_g = 1$ since emboli are weighted in the same direction. The effect of buoyancy is to increase the proportion of ischaemic nodes, which is also a consequence of this weighting. Again, a lack of deformation in emboli leads to near 100% ischaemia. N.B. Results are plotted on a logarithmic scale.

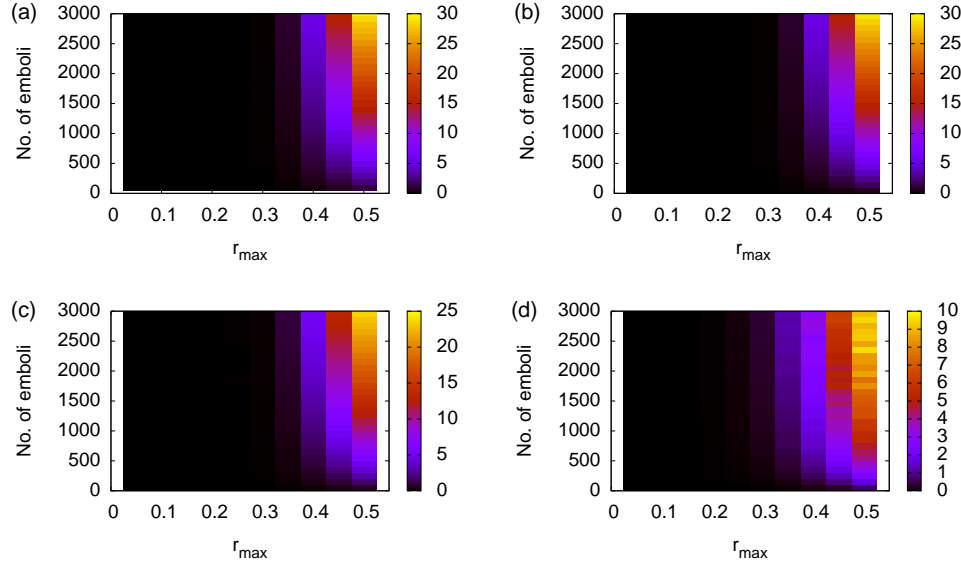


Figure 5. The proportion of end arterioles receiving no supply for 5 minutes when (a) buoyancy is turned off and 1 embolus is produced per second (b) buoyancy is turned off and 0.5 an embolus is produced per second (c) $A_g = 0.5$ and (d) $A_g = 1$. The shape of the graph is similar in all cases, but the proportion of blocked nodes varies dramatically (the colour scales vary between panels). Between panels (a) and (b), the only difference is the rate of embolisation, showing that it is the total number of emboli rather than the exact pattern of embolisation that is most important when the timescale of embolisation is lower than the dissolve time. Panels (c) and (d) show that buoyancy reduces the maximum blockage for the parameters sampled to 25% for $A_g = 0.5$ and to 10% for $A_g = 1$.

is plotted vs time in figure 4. Again several values for the coefficient A_g are shown, and the results for non-deformable emboli are included for comparison. The proportion of nodes that have been ischaemic for at least 10 minutes at some time during the simulation increases monotonically with time and the number of emboli in the shower. It should be noticed that these proportions do not increase linearly, presumably because the same nodes can become ischaemic at a later time in the simulation. This non-linearity is particularly clear for $A_g = 1$ since emboli are weighted in the same direction. The effect of buoyancy is to increase the proportion of nodes that are ischaemic for a long time. A lack of deformation in emboli leads to near 100% ischaemia. This overestimation can also be seen in Fig. 6.

Figure 5 shows the percentage of arterioles subjected to at least 5 minutes of ischaemia for gaseous emboli. Increasing the effects of buoyancy decreases the total percentage of arterioles blocked as the paths of emboli through the tree are restricted by the weighting. Overall, an increase in the maximum size r_{\max} of emboli increases the proportion of arterioles affected by ischaemia. Likewise, increasing the number of emboli in the shower is predicted to increase the proportion of the tree affected by ischaemia. If no blockage is registered, then the cell is black. These calculations demonstrate that a

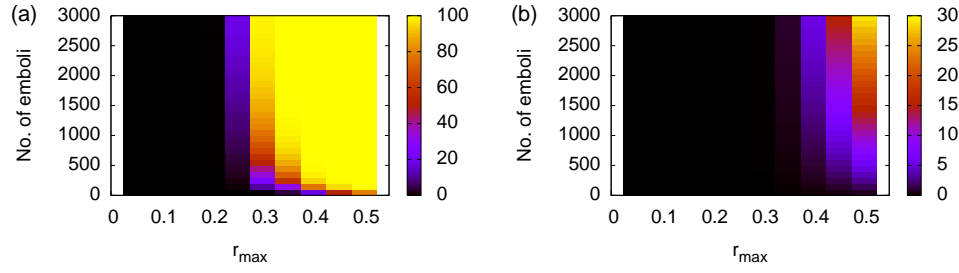


Figure 6. Comparison between the proportion of nodes receiving no blood supply for 5 minutes when (a) emboli are non-deformable and (b) emboli are deformable. Buoyancy effects are not considered. Neglect of embolus deformation in the model leads to a huge overestimation of the proportion of blocked nodes.

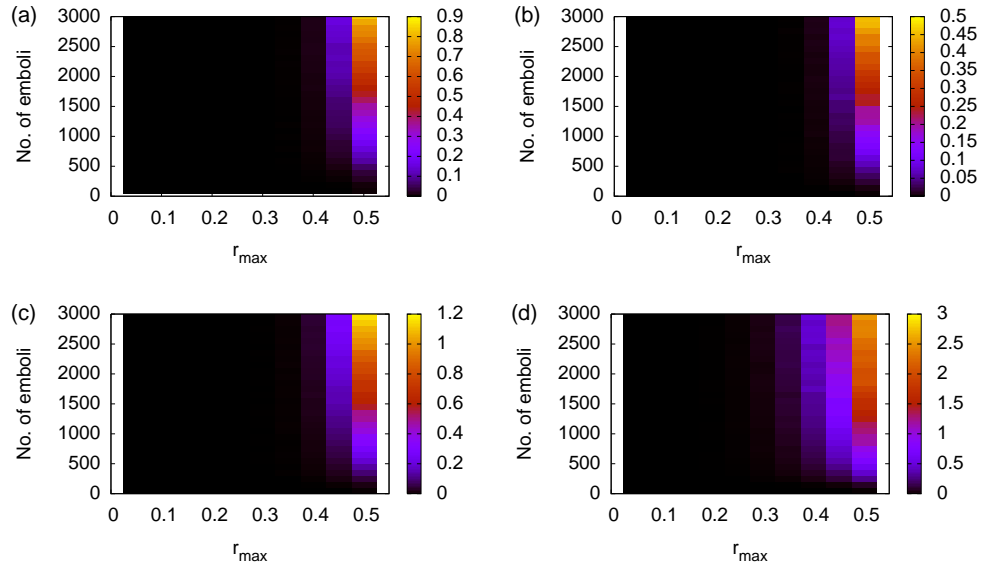


Figure 7. The proportion of nodes receiving no supply for 10 minutes when (a) buoyancy is turned off and 1 embolus is produced per second (b) buoyancy is turned off and 0.5 an embolus is produced per second (c) $A_g = 0.5$ and (d) $A_g = 1$.

smaller number or size of emboli is required to cause ischaemia when emboli are buoyant.

To highlight the differences between deformable and non-deformable emboli, figure 6 shows the proportion of nodes blocked for more than 5 minutes when emboli are (a) rigid and (b) deformable. There are significantly more blockages in the case of non-deformable emboli (in both cases, the same clearance time is used), and this difference persists over all timescales for the ischaemia.

It is of interest to see how ischaemia is affected over longer timescales. Figure 7 (figure 8) shows the percentage of arterioles experiencing at least 10 minutes (15 minutes) of ischaemia. The proportion of arterioles blocked for a longer period of time is around one order of magnitude smaller than the proportion blocked for at least 5 minutes, since the clearance time for a 0.5 mm gaseous embolus is just under 10 minutes [Branger and

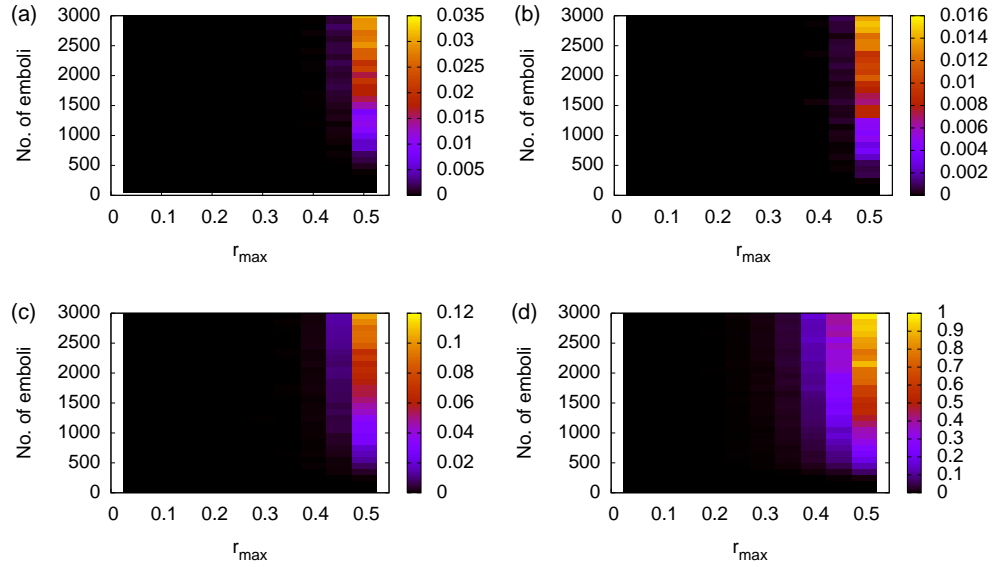


Figure 8. The proportion of nodes receiving no supply for 15 minutes when (a) buoyancy is turned off and 1 embolus is produced per second (b) buoyancy is turned off and 0.5 an embolus is produced per second (c) $A_g = 0.5$ and (d) $A_g = 1$.

Eckmann, 1999] and obstruction from a single embolus drops exponentially with size. Of particular interest is the observation that buoyant emboli produce more persistent blockages (up to 1.8% of arterioles blocked for at least 10 minutes for 1500 gaseous emboli and 0.6% for at least 15 minutes). This is a reversal of the short timescale reduction in blockage, and demonstrates that if emboli have preferred paths through the tree (caused either by topography or buoyancy) their effects are more likely to translate to tissue ischaemia and neuronal injury.

Finally, we discuss two possible mitigation techniques for dealing with gaseous emboli. The first is increase of blood pressure, and the second is the use of CO_2 during surgery. Results for these scenarios can be found in Fig. 9 for emboli of radius up to 0.5mm, and pressures of 100 mmHg and 50 mmHg. Inclusion of pure CO_2 dramatically reduces the blockage, with less than 1% of arterioles blocked on any time step (panel (a)), and with no nodes experiencing ischaemia for ≥ 5 mins, which demonstrates that under ideal conditions, CO_2 insufflation should be effective in reducing the contribution of air bubbles to neurological impairment during cardiac surgery. Another interesting result is the effect of decreased pressure. A drop of the input pressure by a factor of 2 leads to a near doubling in both the number of blocked nodes during embolisation, and in the number of nodes suffering ischaemia for more than 5 minutes. While there may be other good clinical reasons why a lower pressure might be useful on bypass, the results here indicate that maintaining higher pressures may reduce stroke symptoms. The origin of the drop is that the higher pressure can push gaseous emboli further into the tree before they stick, reducing the blockage since the number of nodes downstream from a blockage halves at each bifurcation.

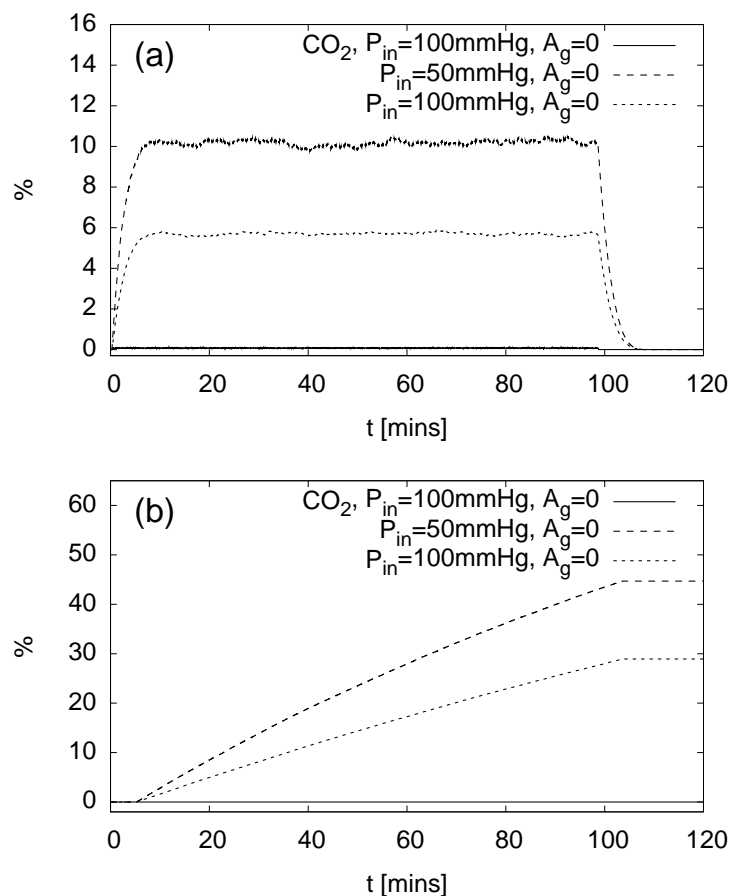


Figure 9. Effect of halving pressure or adding CO_2 on (a) the percentage of blocked nodes and (b) the percentage of nodes that have been ischaemic for at least 5 minutes during the simulation. The results demonstrate that, under ideal conditions, CO_2 insufflation should be effective in reducing the contribution of gaseous emboli to neurological injury during cardiac surgery. A drop of the input pressure by a factor of 2 leads to a near doubling in both the number of blocked nodes during embolisation, and in the number of nodes suffering ischaemia for longer than 5 minutes. N.B. for the CO_2 bubbles, ischaemia did not exceed 5 minutes.

4. Summary

We have investigated ischaemia due to gaseous emboli using an extended model. Our model includes the deformability of gaseous emboli, fluid dynamical considerations and a basic description of embolus buoyancy. We have examined the effects of buoyancy, embolus composition, embolus rate, embolus size, input pressure and the number of emboli in a shower on ischaemia.

We found that deformations of gas bubbles must be considered or blockages in our simulations are vastly overestimated. We also found that gravitational effects reduced the proportion of blocked nodes at a specific time, but slightly increased the proportion of nodes that were ischaemic for an extended period of time. Finally, we discussed two possible mitigation techniques for dealing with gaseous emboli, confirming that under

ideal conditions, CO₂ insufflation should be effective in reducing strokes. We also found that maintaining higher blood pressures in patients on bypass may reduce cognitive decline, with the caveat that it may lead to other clinical complications.

We note that the model still has some limitations. Pulsatile flow has not been considered so far, but flow in the microvasculature is in a near steady state, so the effects of pulsatile flow are likely to be small. We expect to include windkessel equations in a future model to handle pulsatile flow. In our model, gaseous emboli do not split at bifurcations. However, bubble splitting is only likely to affect bifurcations angled within, or close to, the horizontal plane. Finally, our tree is completely symmetric. We are currently in the process of growing realistic cerebral vasculatures *in-silico*.

Acknowledgments

JPH would like to thank EPSRC grant no. EP/H015655/1 for financial support. EMLC is grateful for support from the BHF, grant number FS/10/46/28350.

References

- M. Barak and Y. Katz. *Chest*, 128:291832, 2005.
- A.B. Branger and D.M. Eckmann. *J. Appl. Physiol.*, 87:1287–1295, 1999.
- W.R. Brown, D.M. Moody, V.R. Challa, D.A. Stump, and J.W. Hammon. *Stroke*, 31:70713, 2000.
- F. Cassot, F. Lauwers, C. Fouard, S. Prohaska, and V. Lauwers-Cances. *Microcirculation*, 13, 2006.
- K. Chaudhuri and S. F. Marasco. *J. Card. Surg.*, 26:189–196, 2011.
- E.M.L. Chung, J.P. Hague, and D.H. Evans. Revealing the mechanisms underlying embolic stroke using computational modelling. *Phys. Med. Biol.*, 52:7153–7166, 2007.
- B. Eshpuniyani, J. B. Fowlkes, and J.L. Bull. *Int. J. Heat Fluid Flow*, 26:865, 2005.
- M.D. Georgiadis, M. Kaps, M. Siebler, M. Hill, M. Konig, J. Berg, M. Kahl, P. Zunker, B. Diehl, and E.B. Ringelstein. *Stroke*, 26:439–43, 2005.
- J.P. Hague and E.M.L. Chung. Statistical physics of cerebral embolization leading to stroke. *Phys. Rev. E*, 80:051912, 2009.
- D.M. Moody, M.E. Bell, V.R. Challa, W.E. Johnston, and D.S. Prough. *Ann. Neurol.*, 28:477–86, 1990.
- Y. Abu Omar, S. Cader, L. Guerrieri Wolf, D. Pigott, P.M. Matthews, and D.P. Taggart. *J. Thorac. Cardiovasc. Surg.*, 132:1119–25, 2006.
- A.R. Rodriguez, K.A. Williams, A. Babaev, F. Rubens, and H.J. Nathan. *Perfusion*, 20:3–10, 2005.
- N. Stroobant, G. Van Nooten, Y. Van Bellehem, and G. Vingerhoets. Relation between neurocognitive impairment, embolic load, and cerebrovascular reactivity following on- and off-pump coronary artery bypass grafting. *Chest*, 127:196776, 2005.

- A. Suzuki and D.M. Eckmann. Embolism bubble adhesion force in excised perfused microvessels. *Anesthesiology*, 99:400, 2003.